

# **Fibrin Clot Structure and Mechanics Associated with Specific Oxidation of Methionine Residues in Fibrinogen**

Katie M. Weigandt,<sup>†</sup> Nathan White,<sup>§</sup> Dominic Chung,<sup>‡</sup> Erica Ellingson,<sup>†</sup> Yi Wang,<sup>||</sup> Xiaoyun Fu,<sup>|||</sup> and Danilo C. Pozzo<sup>†\*</sup>

<sup>†</sup>Department of Chemical Engineering, <sup>‡</sup>Department of Biochemistry, <sup>§</sup>Division of Emergency Medicine, and <sup>||</sup>Division of Hematology, University of Washington, Seattle, Washington; and <sup>|||</sup>Puget Sound Blood Center Research Institute, Seattle, Washington

Weigandt et al.

Structure and Properties of Oxidized Fibrin

Submitted August 29, 2012, and accepted for publication October 24, 2012.

\*Correspondence: [dpozzo@u.washington.edu](mailto:dpozzo@u.washington.edu)

## SUPPORTING MATERIALS

### Circular Dichroism

#### Experimental

Oxidized and non-oxidized fibrinogen samples were prepared at a concentration of 0.075 mg/mL and dialyzed into DI-H<sub>2</sub>O for circular dichroism measurements. A Jasco 720 Circular Dichroism Spectrophotometer operated at 25°C is used to obtain circular dichroism spectra over wavelengths spanning between 200 and 270 nm through a 1 mm pathlength quartz cuvette.

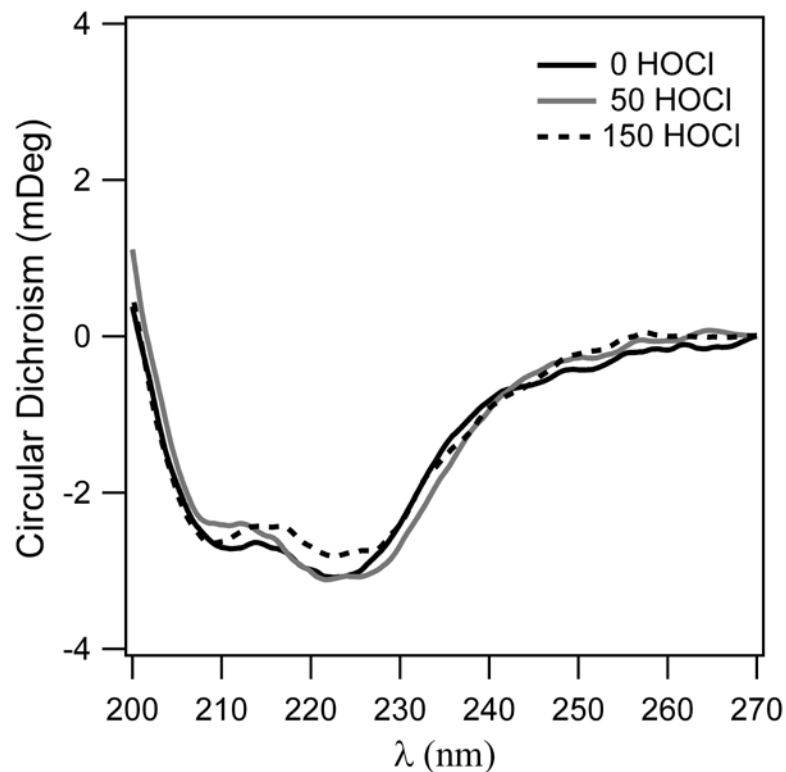


**Figure S1: Circular dichroism spectra from 0, 50 and 150 HOCl fibrinogen at 0.075 mg/mL in water. There is no systematic variation between the baseline and oxidized samples.**

## Scanning Electron Microscopy

Additional Images at 10,000x and 50,000x Magnification

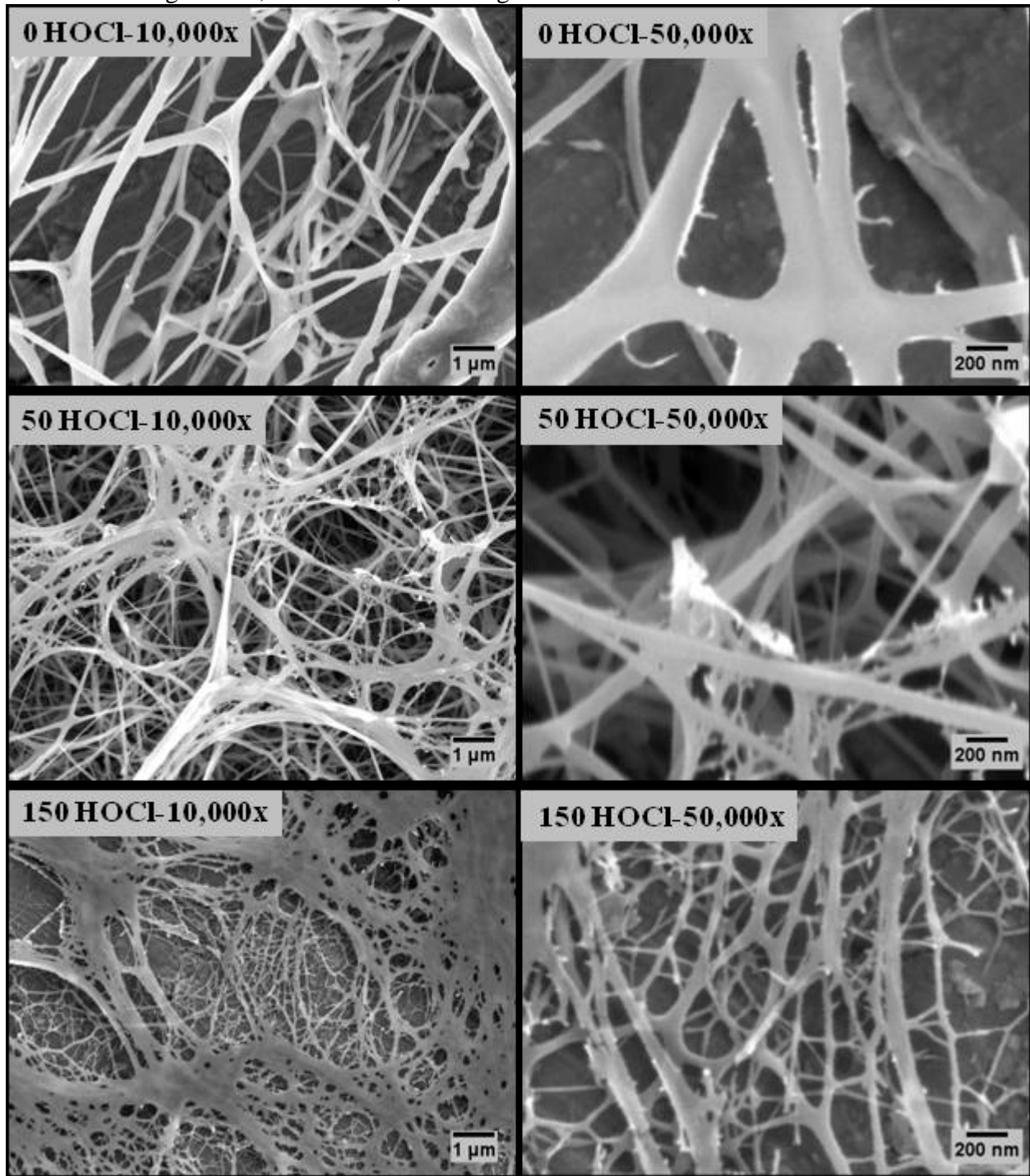


**Figure S2: Supplementary SEM images for 0, 50, and 150 HOCl treated fibrin gels at 10,000 (left) and 50,000x (right) magnification.**

## Turbidity

### Experimental

UV-VIS spectroscopy measurements are made on an Evolution 300 Thermo Scientific UV-visible spectrophotometer. Spectra over  $320 < \lambda < 780$  nm are taken in a 1 cm path length cell once per minute for one hour to capture gelation kinetics and the turbidity of the fully formed gel. Samples are prepared with 1 mg/mL fibrin in the 0.14 M NaCl, 44 mM Hepes buffer with 0.16 NIH u/mL thrombin and 2 mM  $\text{CaCl}_2$ .

### Results

The average fiber diameter can be determined from the wavelength dependent turbidity of the fibrin gel using an analysis described originally by Carr and Hermans or a more recent modified approach described by Yeromonahos et al.[1, 2] The wavelength dependent absorbance of fully formed fibrin gels prepared from fibrinogen of various oxidation levels is plotted in Figure S3 (left). The absorbance of the gels decreases with increasing levels of oxidation. Here we apply Yeromonahos's updated model to determine the fiber diameter from the turbidity of the 0 and 50 HOCl fibrin gels using the wavelength dependent turbidity at  $\lambda > 500$  nm. The 150 HOCl fibrin gel is too translucent to accurately measure the turbidity and is not analyzed with this technique.

First, the turbidity ( $\tau$ ) is determined from the absorbance (A) through a gel of pathlength (L) using the Equation S1:[2]

$$\tau = 1 - \exp(-AL \ln(10)) \quad \text{Equation S1}$$

The turbidity is related to the fiber radius (R) and mass length ratio ( $\mu$ ) using Equation S2.[1, 2]

$$\tau \lambda^5 = \frac{2\pi^3 C n_s \mu}{N} \left( \frac{dn}{dc} \right)^2 \frac{44}{15} \left( \lambda^2 - \frac{184}{154} \pi^2 R^2 n_s^2 \right) \quad \text{Equation S2}$$

Here,  $\lambda$  is the wavelength, R is the radius, C is the fibrinogen concentration,  $n_s = 1.33$ , N is Avagadro's number, and  $dn/dc = 0.176 \text{ cm}^3 \text{ g}^{-1}$ . [1, 2] In Figure S3 (right)  $\tau \lambda^5$  is plotted as a function of  $\lambda^2$ . The radius and mass-length ratio are determined from a linear fit and are listed in Table S1.

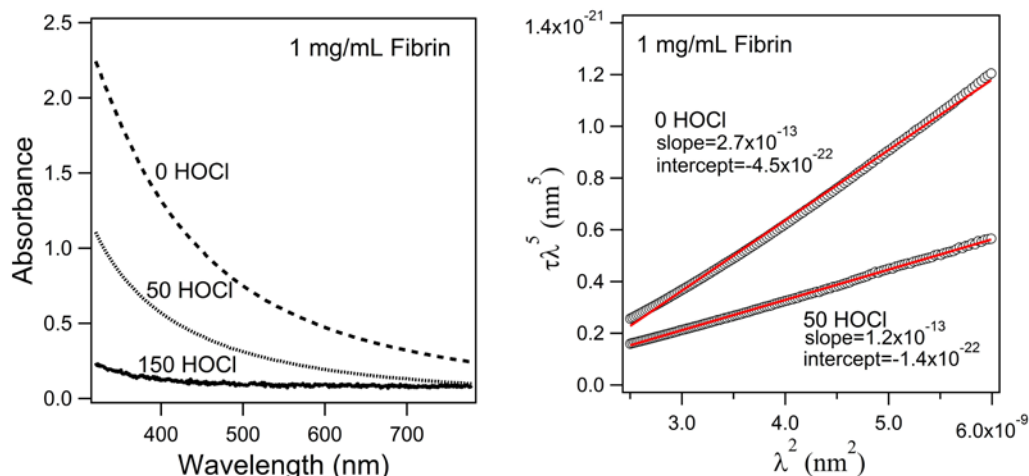


**Figure S3: Left: UV-Vis spectra from the fully formed fibrin gels (after one hour gelation) prepared from 0, 50 and 150 HOCl fibrinogen. Right: Determination of radius and mass-length ratio from turbidity linear fit.[1, 2]**

**Table S1: Fiber diameter and protofibrils aggregation for fibrin gels prepared from 0 and 50 HOCl fibrinogen from turbidity analysis.**

	Radius (nm)	Protofibrils/Cross-section
0 HOCl	89	152
50 HOCl	75	67

## SANS

### Experimental

Baseline and oxidized fibrinogen (0 and 150 HOCl) was used to prepare fibrin gels with the addition of 0.16 NIH units/mL thrombin in a 0.14 M NaCl, 44 mM hepes, 2 mM CaCl<sub>2</sub> buffer at pH 7.4. A relatively high concentration (6.5 mg/mL) of fibrinogen is used to increase the scattering relative to the background. The solution was quickly loaded through an open window in a 4 mm demountable sample cell designed for SANS measurements. Gelation was allowed to proceed for 1 hour prior to additional processing. After gelation was complete, the H<sub>2</sub>O buffer was exchanged with a D<sub>2</sub>O buffer of identical composition in order to enhance the contrast and reduce the incoherent scattering. The buffer was exchanged by topping the gel with the deuterated buffer and allowing the buffer to diffuse into the gel. Three exchanges of the deuterated buffer were performed. The buffer exchange was monitored by measuring the density of the exchange buffer as a function of time. The final solvent isotopic composition was ~96% D<sub>2</sub>O based on density measurements.

Small angle scattering measurements were performed at the NIST Center for Neutron Research in Gaithersburg, MD on the NG7 30 m SANS instrument.[3] Three instrumental configurations were used to cover the full  $q$ -range spanning between 0.0009 and 0.4 Å<sup>-1</sup>. The scattering data was corrected for sample cell scattering and background and placed onto absolute scale relative to the direct beam flux using the NIST Igor based algorithms.[4]

### Results

SANS is used to characterize the structure of fully hydrated baseline and 150 HOCl fibrin gels. The scattering intensity ( $I$ ) is plotted against the scattering vector ( $q$ ) in Figure S3. Here, we observe substantial differences in the scattering from the oxidized and non-oxidized fibrin gels as expected based on the results from the SEM and turbidity studies.

The scattering from the baseline gel is typical for a coarse fibrin clots, with two Porod regions ( $I \sim q^{-4}$ ) that arise from the sharp interface between the protein and the buffer at high- $q$  and the fiber and the buffer at intermediate- $q$ . [5-7] Additionally, at low- $q$  the slope begins to decrease and transition into the  $q$ -range over which the network fractality dominates. This transitional region is the intermediate Guinier region, which is characteristic of cylindrical fibers. The  $q$ -range over which this transition occurs is related to the fiber radius.

The scattering from the non-oxidized gel was fit with the cylinder form factor model defined by Equations S3 and S4 below:[7]

$$I(q) = \phi_f \pi R^2 L (\Delta\rho)^2 P(q) + bkg \quad \text{Equation S3}$$

$$P(q) = \int_0^{\pi/2} \left( \frac{2 \sin\left(qL \cos\frac{\theta}{2}\right) J_1(qr \sin\theta)}{qL \cos\frac{\theta}{2} qr \sin\theta} \right)^2 \sin\theta d\theta \quad \text{Equation S4}$$

where  $\phi_f$  is the volume fraction of fibers,  $q$  is the scattering vector,  $L$  is the fiber length,  $\Delta\rho$  is the scattering contrast and  $\theta$  is the angle of orientation (here an isotropic distribution). The scattering length densities of the solvent and fibrinogen were fixed at  $6.08 \times 10^{-6}$  and  $3.17 \times 10^{-6}$  respectively. Polydispersity in the radius was accounted for using a Schulz distribution with a polydispersity index of 0.3. The scattering in this  $q$ -range is not sensitive to the fiber length, so the length is held fixed at a large value of 1000 nm. The data was fit over a restricted  $q$ -range from 0.0009-0.02 Å<sup>-1</sup>, as the model does not account for the high- $q$  scattering that arises from the internal

structure of the fibers. All model fitting is performed using the DANSE SansView software package.[8] The resulting fit is plotted as a solid line over the 0 HOCl fibrin gel scattering in Figure S4 and the average fiber radius is found to be 95 nm, which is very similar to the 89 nm radius determined through turbidity measurements.

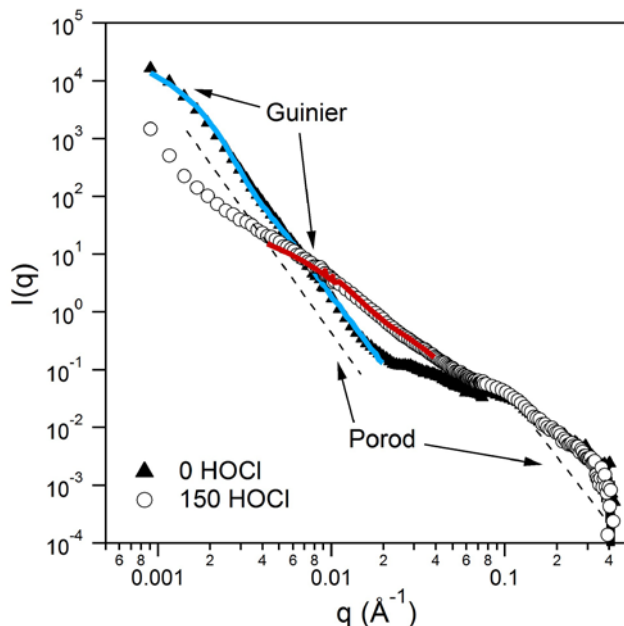


**Figure S4: SANS data from 6.5 mg/mL fibrin gels treated with 0 and 150  $\mu\text{mol}$  HOCl per gram fibrinogen. The data fits using the cylinder and bimodal cylinder models are represented as solid blue and red lines respectively.**

As mentioned above, the scattering from the 150 HOCl gel is dramatically different than the non-oxidized fibrin gel scattering. In the oxidized gel, the Guinier transition corresponding to the fiber diameter occurs at about an order of magnitude higher- $q$ , which is indicative of a substantially reduced fiber diameter. Additionally, there is no clear Porod region separating the internal structural features from the cross-sectional Guinier, suggesting that the fibers may have a broad or perhaps even bimodal distribution in the fiber radius.

The 150 HOCl gel is not well represented by a single polydisperse cylinder model. Instead, this data is well fit with a bimodal distribution of cylinders by summing the form factors of two polydisperse cylinders (Schulz distribution, PDI=0.3). As with the baseline gel, the polydispersity, scattering length densities, and fiber length are held constant. Here, the data is fit over a limited  $q$ -range between  $0.004 < q < 0.04 \text{ \AA}^{-1}$ . The resulting fit is plotted over the 150 HOCl scattering curve in Figure S4, with the best fit found with average radii at 15 and 3.4 nm. While the fit was very good, there is significant uncertainty in the absolute value of the radii. In fact, the small radius determined from the fit is slightly less than what is expected for a single protofibril ( $\sim 5 \text{ nm}$ ).<sup>[9]</sup> However, these results are consistent with the SEM images where there is a clear reduction in size and where both very small and slightly larger fibers are observed in the oxidized sample.

## SDS-PAGE

### Experimental

Oxidized and non-oxidized fibrinogen samples (0.4 mg/ml) were converted to fibrin by either thrombin (0.4 unit/ml, Hematologic Technologies Inc.) or reptilase (4  $\mu$ g/ml, Prospec) in 50 mM Hepes, pH 7.4, 2 mM  $\text{CaCl}_2$  and 0.14 M NaCl, for 15 min at 22 °C. Fibrinogen and fibrin samples (15  $\mu$ l) were reduced with 0.18 M mercaptoethanol in the presence of 2% SDS at 100 °C for 1 min, and analyzed on a 4-15% gradient polyacrylamide gel (Bio-Rad) in the discontinuous buffer system of Laemmli.[10] The gel was washed for 15 min in deionized water, stained with Gel Code Blue (Thermal Scientific), and destained in water.

### Results

A scanned image of the PAGE gel that oxidized and non-oxidized fibrin is plotted in Figure S5. The separated protein bands are identical in columns two and four, which correspond to baseline and oxidized fibrin gelled for 15 minutes in the presence of thrombin. The 115 kDa  $\gamma$  dimers( $\gamma_2$ ) are prominent in both the oxidized and fibrin separations and are indicative of covalent cross-linkage via Factor XIIIa. This is clear evidence that Factor XIIIa activity is not impaired by HOCl oxidation.

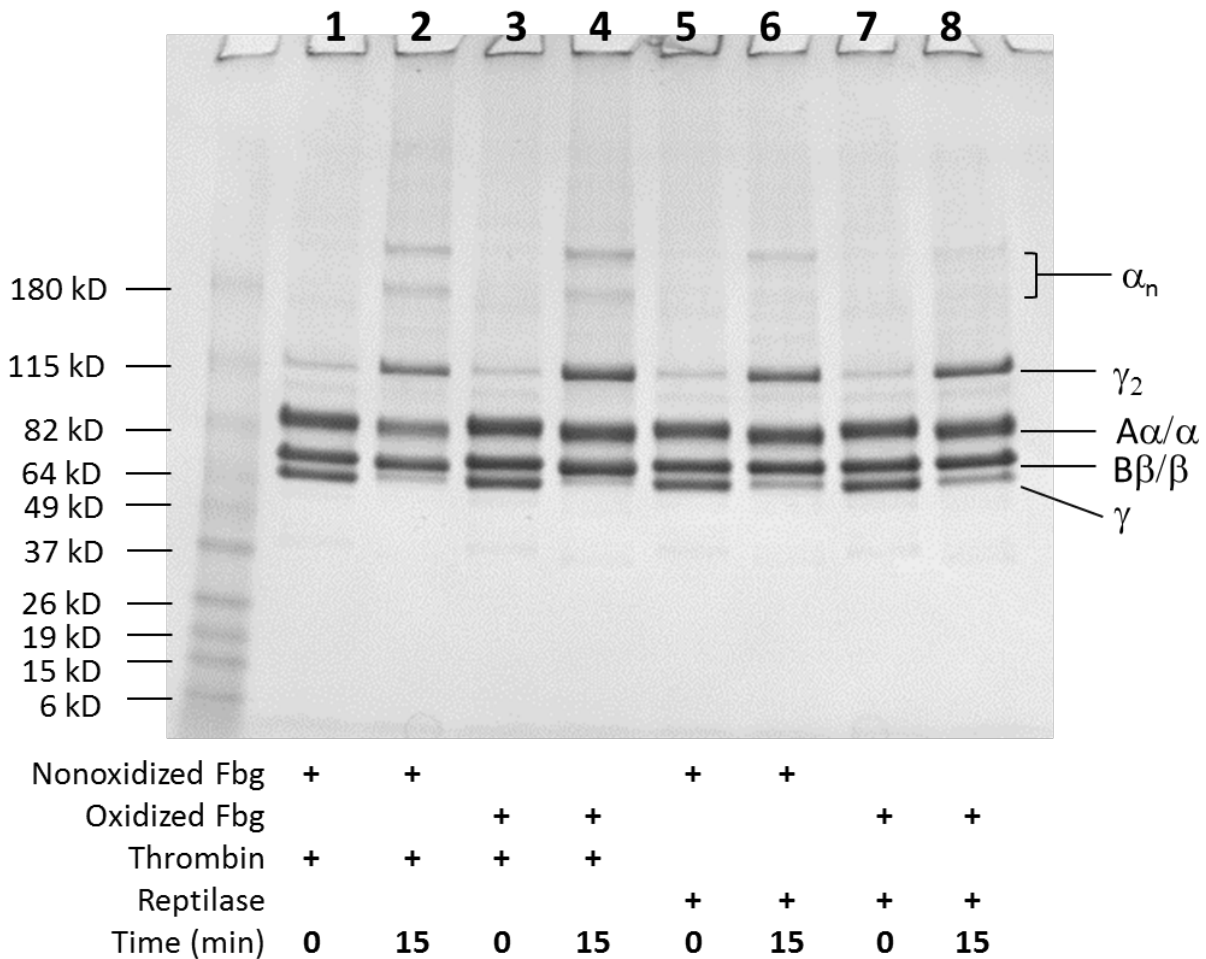


**Figure S5: Scan of gel from SDS-PAGE of oxidized and baseline fibrin.**



## Rheology

### Experimental

Fibrin gels were formed from 0, 50 and 150 HOCl fibrinogen at 1 mg/mL in a 0.14 M NaCl, 44 mM HEPES buffer with 2 mM CaCl<sub>2</sub> and 0.16 NIH u/mL thrombin. Gelation was monitored with 0.5% strain oscillations at one Hz for one hour (plotted in Figure 4 of the main text) and subsequently frequency sweeps were performed over 0.0005 < f < 50 Hz at 0.5% strain. The results of the frequency sweeps are plotted below in Figure S6.

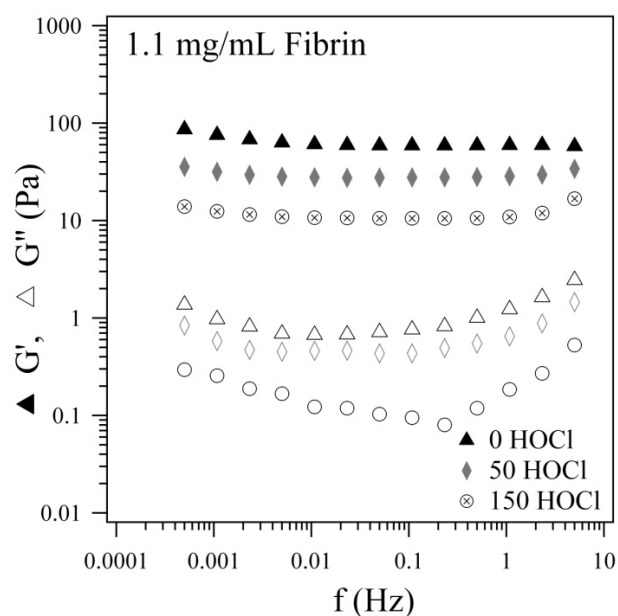


**Figure S6: The elastic ( $G'$ ) and viscous ( $G''$ ) moduli of fully formed baseline and oxidized fibrin gels are plotted as a function of oscillation frequency.**

- [1] M. E. Carr, and J. Hermans, *Macromolecules* **11**, 46 (1978).
- [2] C. Yeromonahos, B. Polack, and F. Caton, *Biophysical Journal* **99**, 2018 (2010).
- [3] C. J. Glinka *et al.*, *J. Appl. Crystallogr.* **31**, 430 (1998).
- [4] S. R. Kline, *J. Appl. Crystallogr.* **39**, 895 (2006).
- [5] K. M. Weigandt, L. Porcar, and D. C. Pozzo, *Soft Matter* **7**, 9992 (2011).
- [6] K. M. Weigandt, L. Porcar, and D. C. Pozzo, *Soft Matter* **5**, 4321 (2009).
- [7] O. Spalla, *Neutrons, X-rays, and Light: Scattering Applied to Soft Condensed Matter* (Elsevier, Amsterdam, 2002).
- [8] DANSE, (2012).
- [9] P. A. Janmey, J. P. Winer, and J. W. Weisel, *Journal of the Royal Society Interface* **6**, 1 (2009).
- [10] U. K. Laemmli, *Nature* **227**, 680 (1970).